Proceedings of the ASME 2020 15th International Manufacturing Science and Engineering Conference
MSEC2020
June 22-26, 2020, Cincinnati, OH, USA

MSEC2020-13235

EXPERIMENTAL STUDY ON COST-EFFECTIVE ADDITIVE MANUFACTURING OF SILICA AEROGEL

Zipeng Guo
Industrial and Systems Engineering Department
University at Buffalo, the State University of New York
Buffalo, NY, 14260

Ruizhe Yang
Mechanical and Aerospace Engineering Department
University at Buffalo, the State University of New York
Buffalo, NY, 14260

Tianjiao Wang
Industrial and Systems Engineering Department
University at Buffalo, the State University of New York
Buffalo, NY, 14260

Lu An
Mechanical and Aerospace Engineering Department
University at Buffalo, the State University of New York
Buffalo, NY, 14260

Shenqiang Ren
Mechanical and Aerospace Engineering Department
University at Buffalo, the State University of New York
Buffalo, NY, 14260

Chi Zhou[1]
Industrial and Systems Engineering Department
University at Buffalo, the State University of New York
Buffalo, NY, 14260

ABSTRACT

The conventional manufacturing process of aerogel insulation material relies largely on the supercritical drying, which suffers from issues of massive energy consumption, high-cost equipment and prolonged processing time. With the consideration of large market demand of the aerogel insulation material in the next decade, a low-cost and scalable fabrication technique is highly desired. In this paper, a direct ink writing (DIW) method is used to three-dimensionally fabricate the silica aerogel insulation material, followed by room-temperature and ambient pressure drying. Compared to the supercritical drying and freeze-drying, the reported method significantly reduces the fabrication time and costs. The cost-effective DIW technique offers the capability to print complex hollow internal structures, coupled with the porous structure, is found to be beneficial to the thermal insulation property. The addition of fiber to the ink assures the durability of the fabricated product. The foam ink preparation methods and the printability are demonstrated in this paper, along with the printed samples for characterizing thermal insulation performance and mechanical properties.

Keywords: Additive Manufacturing, Thermal insulation material, Direct ink writing, Low-cost fabrication.

1. INTRODUCTION

Aerogel as a multiscale solid structure with ultra-high porosity and low density is a preferable material for thermal insulation purposes. Aerogel has strategical importance in wide-spreading applications including construction and architecture [1, 2], aerospace and automobile [3], energy conversion and storage industries [4], etc. Among various thermal insulation materials, silica aerogels exhibit the lowest thermal conductivity compared to any other structures known so far, at a level of 0.015 W/m·K at ambient temperature [5]. The commercially available aerogel products from Aspen [6, 7] and Cabot [8] offer thin (5-10 mm thickness), hydrophobic, sound-proof and flexible aerogel insulation sheets. These products are synthesized by the approach of supercritical condition drying [9]. The supercritical drying is a common approach to fabricate aerogel by removing the low surface tension liquid from the silica skeletons, with the help of supercritical CO_2 or CH_4 to make crack-free aerogel. Due to the prohibitively expensive equipment and time cost, aerogel production on an industrial scale however remains largely limited. It is anticipated to cost $7.2 per square-meter of silica aerogel sheet (3 cm thick) produced [10]. Furthermore, the

[1] Corresponding author: chizhou@buffalo.edu

drying cost increases exponentially with the increasing sheet thickness.

Alternative approaches to fabricate aerogel include freeze-drying and ambient drying. Though the freeze-drying lowers down the cost of fabrication, it suffers from the scalability issues including high-cost, low-efficiency and small-dimension. The conventional ambient pressure drying process is a less energy intensive approach. The organic solvents are used in the precursor gel, such as hexane, heptane and octane, etc. Due to their low surface tension during the ambient drying process, this method is also applicable for making crack-free aerogels. However, it usually leads to the generation of hydrochloric acid, which needs to be further removed by other organic solvents[11, 12]. The use of large amount of organic solvents makes it challenging for large-scale production and real-world applications.

Researchers have also been exploring additive manufacturing or 3D printing, as an advanced manufacturing technique to fabricate complex structure objects, and print aerogels with porous structures. Owing to the unique layer-by-layer fabrication concept, 3D printing is capable of manipulating the hierarchical structure both internally and externally. The 3D printing techniques bring huge potential to produce highly customized aerogel products with intricate macroscale architecture and microscale structure in the same time. Among various 3D printing processes, the drop-on-demand inkjet printing has been used to print graphene oxide ink into a truss structure and also print ice to support the bridges above the hollow regions. The building environment has the temperature well below the freezing point [13-17]. The printed ice will be further removed by freeze-drying process, leaving an ultra-low-density graphene oxide network. In this case, the freeze-drying serves as an indirect way to produce the internal porous structure.

The direct ink writing has been used to fabricate hybrid silica aerogel [18], the hybrid silica aerogel is made by assembling the silk fibroin biopolymers inside the silica structure to make the structure flexible, compressible and fire retardant. The ink shows good printability and the direct ink writing can print parts with customized morphology and microstructures. After printing, the sample was put into oven for the sol-gel reaction/gelation and then dried using the supercritical CO_2 drying. Other researchers have been trying a direct way to generate the porous structure. Towards direct printing a hierarchical cellular structure with low-density and high-porosity structure, a direct foam writing technology was reported by Muth. et al. [19]. A viscoelastic foamed ink was designed, the air bubbles inside the ink formed a stable bubble microstructure and retained the bubble characteristic content and size over a long period of time. The foam ink was then used to directly print the objects and sintered to fabricate high-porosity, mechanically strong structures. Compared to the inkjet printing technique, this approach can achieve scalable fabrication of porous materials, and has large potential applications in thermal insulation. The printed sample undergoes a set of sophisticated drying procedures, including a humidity-controlled and a series of sintering treatments. Despite the fact that these methods are capable of fabricating porous and mechanically strong aerogels, the processing time is a bottleneck for producing large-scale aerogels.

Taking the advantage of printing complex internal structures in three dimensional space, it could potentially save the material by designing the hollow internal structure and also tuning the

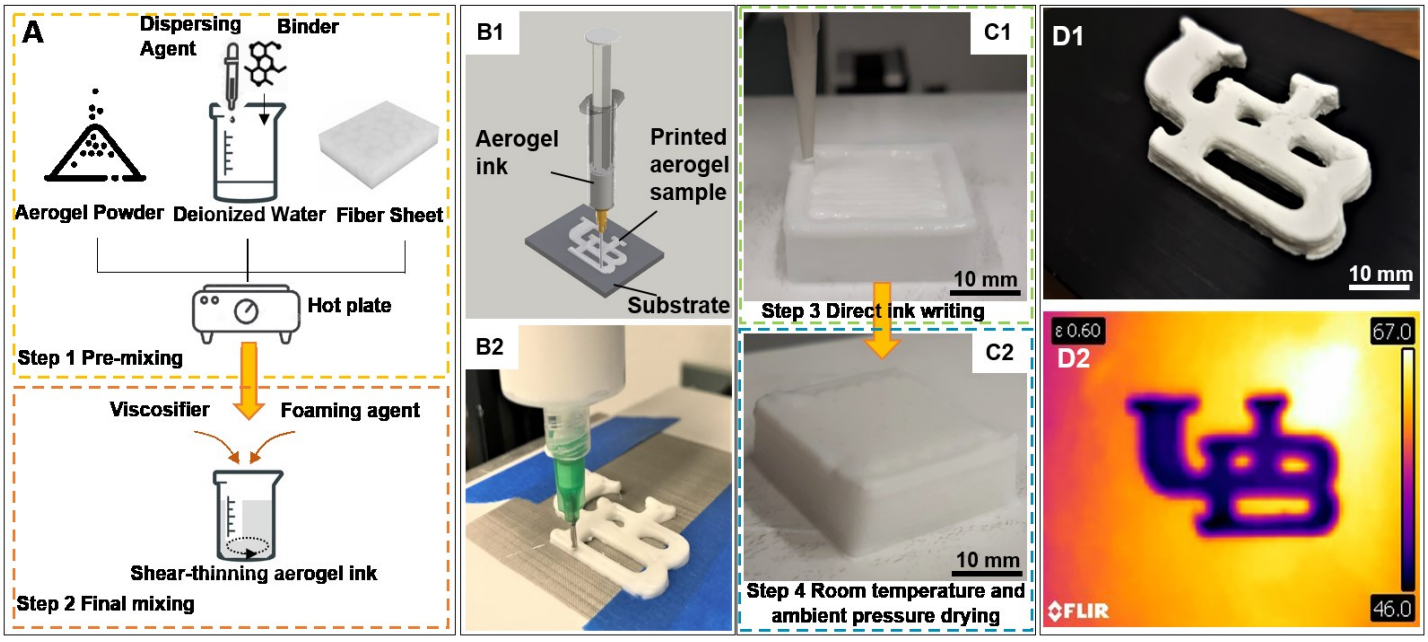

FIGURE 1: Direct ink writing of silica aerogel insulation material. A) Printable ink preparation. B1) Schematic of direct ink writing of University at Buffalo (UB) logo. B2-B3) Direct ink writing process. B4) Ambient pressure drying of printed sample. C1) UB-logo sample after drying. C2) Infrared image of UB-logo sample on hotplate.

infill density. Coupling with ambient pressure drying, which can in-situ generate the porous structure, the integrated process has the potential to scale-up the manufacturing process by significantly reducing the monetary cost and time cost. In this regard, we propose to combine the direct ink writing and ambient pressure drying to 3D print silica aerogel insulation material. While it is challenging to have a good thermal insulation behavior as well as maintain mechanically strong property for the high-porosity structure. Herein, a direct ink writing technique combined with ambient pressure drying approach, as a cost-effective production method, is demonstrated. The innovation of this approach is the cost-effective in-situ porous generation process and the durable pore-supporting structure with the help of additives, such as the foaming agent and fiber. When the foaming agent contacts with the silica gel precursor, it will spontaneously react with the precursor and generate carbon dioxide in-situ. The formed carbon dioxide gas will be trapped in the precursor, with the pressure in the resulting bubbles opposing the capillary pressure, which prevents the pore shrinkage or collapse during the ambient pressure drying process. Compared with the supercritical point drying, where the pores are produced by removing the solvent using the precise and expensive equipment, our reported ambient pressure drying approach can significantly reduce the energy, time and cost. To facilitate printing in three-dimensional (3D) space with customized structure, the 3D printable ink with embedded gaseous bubbles is designed. Based on the precursor, a few additives are added to modify the rheological properties of the ink. Specifically, the cellulose-based viscosity modifier can make the ink viscous enough, in order to have a shear-thinning behavior. The highly viscous and shear-thinning non-Newtonian fluid is ideal for printing high quality surface finishing specimens. Fiber is added to the ink to reinforce the mechanical strength. To make smooth and continuous ink, the blending procedure (introduced in Section 2.1) is also designed for each batch of chemicals adding to the ink. As shown in Figure 1 (A), the diagram illustrates the procedures of preparing the printable ink, three steps of blending are required. The blending of the fiber content assures no large or tangled fibers are included in the ink. The subsequent procedure of pre-mixing the precursor is used to uniformly distribute the solid particles in the solvent. After adding the viscosity modifier, a finial blending provides the ink with shear-thinning property. Then foaming agent is added and followed by vigorously blending to generate bubbles. While inappropriate blending process will result in non-uniform extrusion or nozzle-clogging during the printing process. After the preparation of ink, it is loaded into a custom-assembled 3D printer, the printing job file is prepared by generating G-code of the 3D geometry. Figure 1 (B1) is a schematic drawing to demonstrate the printing process, (B2) is the image captured during the printing process. Different 3D structures are printed to demonstrate the printability, shown in Figure 1 (B4) as a cuboid and (C1) is the logo of the University at Buffalo (UB). As introduced, after printing the UB logo, it was dried in an ambient pressure environment. Figure 1 (C2) is an infrared image as a demonstration of the thermal insulation property of the UB logo. The base-plate temperature is 67^{O}C, the top surface of the UB logo is 46^{O}C. The image is captured after 30 minutes of heating. The temperature difference of the bottom plate and top surface of the logo shows an effective thermal insulation, and the uniform color of the logo shows good integrity of the printed specimen.

The following experimental study is firstly performed to study the thermal insulation behavior with respect to different drying method, namely, freeze drying, sintering and ambient pressure drying. It is aimed to demonstrate the ambient pressure drying can result in a same level of thermal conductivity performance while it can substantially cut down the drying process time and cost. Then the compression tests are performed for the direct-ink-printed, near-net-shape, crack-free samples to characterize the mechanical property. Finally, the infill density, fiber content and foaming agent content, as three of the major process parameters, are studied to provide a guidance on the optimization of the printing process to reach an optimum pore size controlling and thermal insulation property.

The remainder of this paper is organized as follows: In section 2, the printable ink preparation, printing process and drying methods are introduced, the printability of the prepared ink is also discussed. Section 3 demonstrates a comparison of drying methods to verify the cost-effectiveness of the proposed ambient pressure drying process, along with the characterization of the printed specimens. Section 4 is a comprehensive discussion of the results. Conclusion and future work are presented in Section 5.

2. MATERIALS AND METHODS

2.1 Printable ink preparation

The printable ink in general shall have the rheological behavior of highly viscous and shear-thinning non-Newtonian fluids. The ink preparation is critical for ensuring the printing quality. Beginning with the aerogel powder, a few additives are added to tailor the rheological properties.

The ink is prepared by firstly mixing aerogel powder into the solvent at a concentration of 60wt.%. The solvent is made by dissolving Polyvinyl alcohol (PVA, Mw~10,000, Sigma-Aldrich, St. Louis, MO) into deionized (DI) water at a concentration of 0.05 gram/mL of the DI water. PVA serves as the binder to improve the strength and integrity of the printed sample. The good integrity also makes the printed sample less dusty after drying. Darvan 811(Vanderbilt Minerals, Norwalk, CT) is added by 1.6 vol% of the DI water to disperse the aerogel powders. The commercially available Fiber sheet (E08, Unifrax, Buffalo, NY) is blended using a food blender (BBR-2001, Capbran Holdings, Los Angeles, CA), then added to the prepared solvent by 10 wt.% of the aerogel powder. The suspension is pre-mixed homogenously for 6 hours on a magnetic stirring hot plate (UX-04600-12, Thermo Scientific, Waltham, MA). Hereafter, Hydroxypropyl methyl cellulose (HPMC, H7509, Sigma-Aldrich, St. Louis, MO) is added to the suspension as a viscosity modifier at a concentration of 12 mg/mL of the DI water. HPMC

will be equally split to two batches, adding to the suspension sequentially. The first batch is added and followed by blending for 3 hours, then the second batch is added and again blended for 3 hours. Sequentially adding the HPMC will help it thoroughly

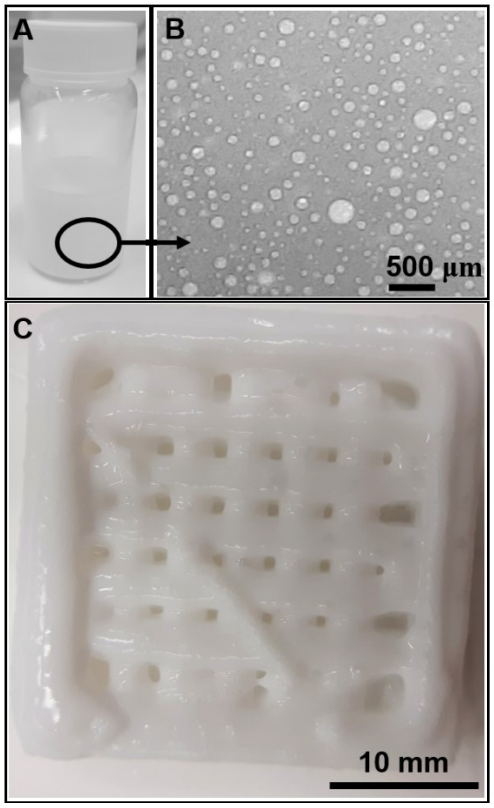

FIGURE 2: Printable ink and Printability. A) Foamed ink. B) Gaseous bubble inside of the paste. C) Printing sample with 80% infill pattern.

dissolved into the suspension, whereas directly adding the entire batch will cause HPMC to tangle together. Finally, Cetyltrimethylammonium bromide (CTAB, VWR, Radnor, PA) is added as the surfactant to form uniformly distributed gaseous bubbles, which will be developed into the porous structure after printing. Unlike the conventional way to make printable ink, where a defoamer chemical such as 1-Octanol is added to make smooth and continuous paste (slurry) [20, 21], the proposed approach in this work took the opposite route by adding foaming agent to generate pore-supporting porous structure. With the presence of defoamer, the printed sample using traditional approach will have a good integrity, but essentially result in dense structure, which is not ideal for thermal insulation purposes. Here the CTAB takes an opposite effect in the ink, as a foaming agent, which generates the bubbles by vigorously blending for 30 minutes. Bubbles retain the size and quantity after one week of aging in a closed container. Figure 2 (A) shows the ready-to-print ink, (B) is a sub-figure of close-up view of the ink, the gaseous bubbles are evenly distributed in the ink.

2.2 Ink printability

To achieve a continuous and stable extrusion of the ink, the effective printing speed (v_{eff}) is calculated by [19]:

$$v_{eff} = \frac{Q}{\pi(d/2)^2} \quad (1)$$

Where, Q is the volumetric flow rate, which is measured as 9.05 mm^3/sec. d is the nozzle inner diameter, a 1 mm diameter nozzle is used to print all the samples for characterization, which corresponds to an effective print speed of 8 *mm*/*sec*. Faster printing speed will result in non-continuous filament extrusion, while slow speed will cause over extrusion.

2.3 Direct writing of silica aerogel ink

A custom-assembled 3D printer is constructed, the screw-driven linear stage (Velmex XN10, Bloomfield, NY) is mounted onto the printer, this linear stage provides mechanical force for extruding the aerogel ink. As the stage moves down, a downward mechanical force will be generated, which then exerts on the piston of the syringe, pushing it downwards, and extruding the ink out of the nozzle. The prepared ink is loaded into a 30 mL syringe with a helix-locked conical shape nozzle (Nordson EFD, East Providence, RI) attached to the tip of the syringe. The nozzle has an internal diameter of 1.0 mm. The extruder path and G-code are generated by Slic3r software (slic3r.org), the infill pattern is set as rectilinear, layer thickness is 0.8 mm. As a process parameter that can only pertain to 3D printing process, the infill density is set at 50%, 75% and 100%, respectively, which is used to study its influence on the thermal conductivity. The result is shown in the next section. A stainless-steel woven mesh-sheet (SATINIOR-Woven-02) is used as a substrate, the fine meshes on the thin sheet is permeable to air, which prevents the printed sample from cracking caused by non-uniform drying. In addition, the flexible mesh sheet can be easily peeled off from the sample without damaging the bottom surface. Figure 2 (C) shows the printing sample with an 80% infill density, the rectilinear infill pattern is adopted. Two perimeter shells are firstly printed, the perimeter shells are in solid-infill, it forms the overall shape of the sample, then the internal potion of the sample is filled using the rectilinear pattern, which turns out to have the best printing quality.

2.4 Ambient pressure drying

Once printed, the samples are dried in an ambient pressure and room temperature environment. After 6 hours drying, the mesh substrate can be easily peeled off from the sample. With additional 4-hour drying, the as-printed solid sample is obtained. The samples have a thickness of ~8mm, and the drying time linearly proportional to the thickness.

3. CHARACTERIZATIONS AND RESULTS

3.1 Drying methods comparison

To verify the ambient pressure drying is a cost-effective drying method for producing the highly porosity silica aerogel insulation material, three different drying methods are compared, namely freeze-drying, sintering and ambient pressure drying. The sample for this set of tests are cubic shapes with dimension of 30mm length by 30mm width by 8mm in thickness.

To perform the freeze-drying method, the printed cubic samples are firstly put into a refrigerator with a -20^{O}C chamber. The primary drying process starts from -40^{O}C, ramped to -10^{O}C at a rate of 0.25 ^{O}C/min, and held at -10^{O}C for 6 hours. Followed by the secondary drying process starts from -10^{O}C, warm up to 0^{O}C at a rate of 0.25 ^{O}C/min, and held at 0^{O}C for 6 hours. Finally, the chamber temperature is elevated to 20^{O}C at the rate of 0.25 ^{O}C/min and hold for 2 hours, to allow the solvent content to be completely sublimated. The vacuum of the system is maintained at 0.013-0.018 mBar during the entire drying process. The processing time is 23 hours in total.

The sintering method aims to burn out the organic component inside the sample, left with the empty pore structure. The printed

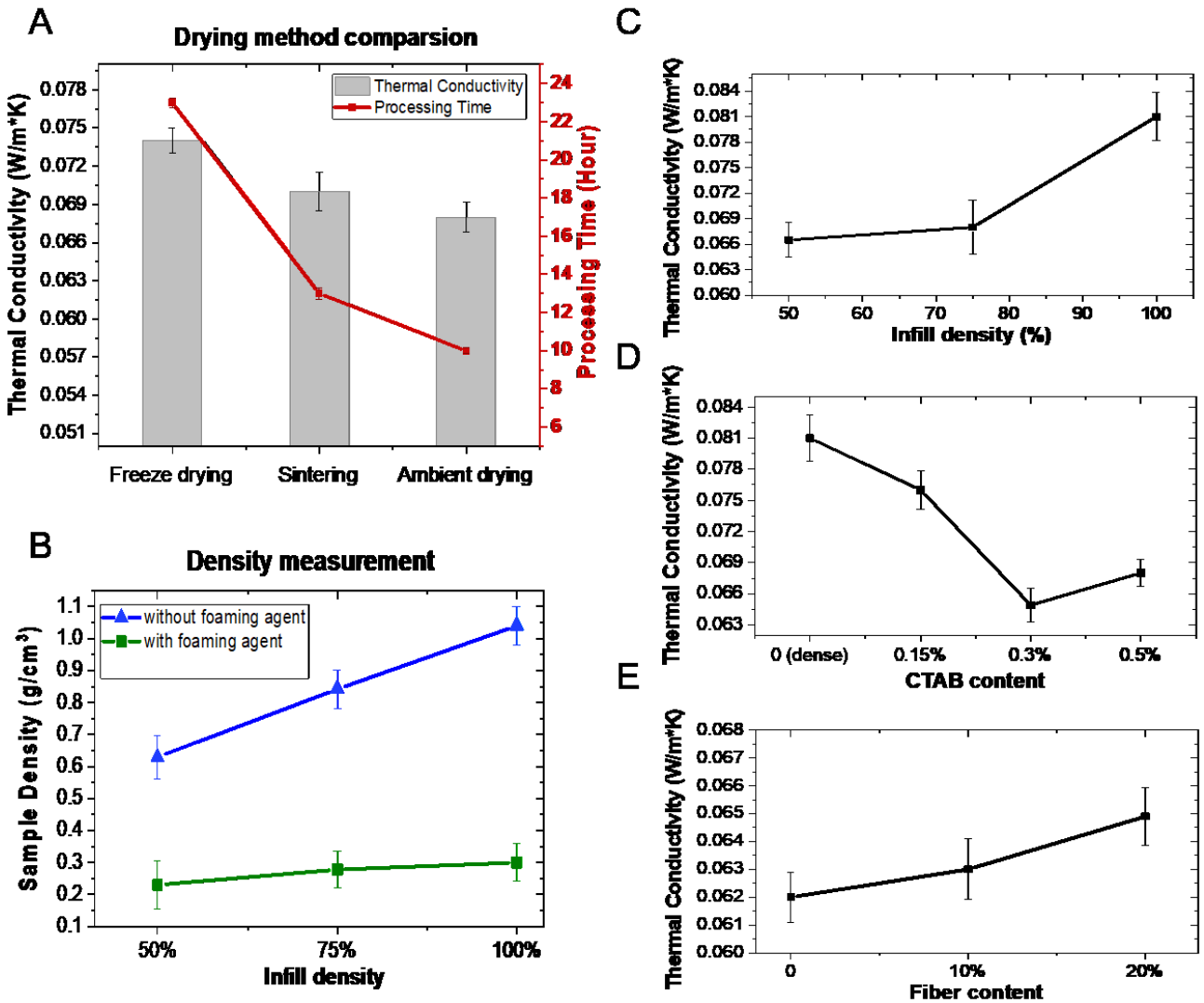

FIGURE 3: Cost-effective ambient pressure drying and characterization results. A) Comparison of freeze drying, sintering and ambient drying with respect to the thermal conductivity. B) Density measurement of samples without surfactant and with surfactant. C) Study the effect of infill density on the thermal conductivity. D) Study the effect of CTAB content on the thermal conductivity. E) Study the effect of fiber content on the thermal conductivity.

environment to freeze the sample. The freeze-drying system (FreeZone Triad Model 7400 Series, LABCONCO, Kansas City, MO) is pre-frozen to -40^{O}C, then the sample is put into the sample is firstly dried in room temperature for 6 hours, after the substrate is removed from the sample, then transferred into a tube furnace (GSL-1500X, MTI Corporation, Richmond, CA). The

heating profile begins from room temperature, then ramps up to 400^{O}C at a rate of 2 ^{O}C/min, and holds for 2 hours at 400^{O}C, followed by natural cooling to room temperature. The processing time is 13 hours in total.

As described in Section 2.4, the room-temperature ambient pressure drying takes 10 hours in total.

After the samples are dried using three different methods, the thermal conductivity is measured by a custom-built heat flux sensing instrument, which is composed of a heated plate at the top and a cooled plate at the bottom, with two heat flux sensors attached to each plate. The temperature of the heated plate remains constant at 37 ^{O}C, and the temperature of the cooled plate was set at 30^{O}C. The sample is placed in between the two heat flux sensors. The heat flux and thermal conductivity relationship is given by

$$q = \frac{-\lambda * \Delta T}{\Delta x} \quad (2)$$

where q is the heat flux value collected by the sensors, λ is the thermal conductivity, ΔT is the temperature difference across the sample collected by the embedded thermal couple in the sensors, and Δx is the thickness of the sample. In general, the negative sign is an indication of the direction of the heat transfer.

The results are shown in Figure 3(A), it confirms the hypothesis that three different drying methods reach the same level of thermal insulation performance, with the ambient pressure drying has the lowest thermal conductivity, and the freeze drying has the highest thermal conductivity. Further considering the processing time, freeze drying takes more than twice of the time compared to the ambient pressure drying. It is sufficient to conclude that ambient pressure drying is effective for 3D printing of silica aerogel insulation material with low-cost.

3.2 Density measurements

Considering all the characterization samples are in bulk cubic structures, the relative density is calculated according to the mass and volume of the sample. Mass is measured by a weighting scale (AX223, OHAUS, Parsippany, NJ). Two sets of samples are compared, one set are the dense samples, where no surfactant is included in the ink recipe, resulting in very limited pores in the sample. While the other set of samples are considered as porous samples, where the CTAB concentration is 0.5 wt.% of the aerogel powder. CTAB as the agent to generate gaseous bubbles in the ink, will be further developed into the porous structures. As is shown in figure 3(B), three different sets of infill density are applied to the samples. With the presence of surfactant, the sample density is reduced to one-third of the dense samples, meaning CTAB plays an important role in generating the porous structures, which is critical for thermal insulation behavior.

3.3 Thermal conductivity measurements

Thermal conductivity is one of the key factors for thermal insulating property. To investigate the relation between the process parameter and the thermal conductivity, three sets of experiment are studied, namely, infill density, CTAB content and fiber content.

The infill density describes the amount of ink printed inside the object, which can be precisely designed and controlled in additive manufacturing. Less infill density results in saving material and short printing duration. Three infill-densities are compared, 50%, 75% and 100%, respectively. The result is shown in Figure 3(C), the fully filled sample has the highest thermal conductivity, while the 50% infill samples reach the lowest thermal conductivity with a 20% reduction. The result concludes that relatively less infill density benefits the thermal insulation property. Consider a 50% infilled sample, the other 50% is left as empty pores, and the pattern is precisely controlled by the printing process, together with the micro-pores generated by the surfactant, which makes it less conductive to the heat.

The effect of CTAB content on the thermal conductivity is studied in order to find an optimum value to reach the best insulation performance. Four contents are compared, 0 wt.%, 0.15 wt.%, 0.3 wt.% and 0.5 wt.% concentration, respectively. As indicated in Figure 3(D), the dense sample has the highest thermal conductivity, while the 0.3 wt.% concentration sample has the lowest value. Further increase of the concentration will result in the increase of the thermal conductivity again. It is reasonable that for the dense sample, due to the very limited pores inside of the sample, the conductivity is high. With the presence of CTAB, the generated pores help to lower down the conductivity. While the reason that 0.5 wt.% concentration sample has higher conductivity compared to the 0.3 wt.% is due to the excessive CTAB tends to over generate bubbles. The over generated small bubbles will combine together to large bubbles in an uncontrolled form, resulting in large pores inside the sample. When the heat transfers from the bottom, the air molecules carry the heat and quickly pass through the large empty pores without any resistance, then the heat is easily transferred to the top surface. The ideal pore structure would be uniformly distributed pores with controlled size and pattern [22].

The fiber is added to the ink for the consideration of the mechanical strength of the printed sample. To verify the hypothesis that fiber reinforces the sample, but not affects too much on the thermal conductivity, three different fiber contents are studied, 0 wt.%, 10 wt.% and 20 wt.%, respectively. The result is shown in Figure 3(E), the change of fiber content does not cause the thermal conductivity fluctuate too much, with a maximum value of 0.0649 W/m*K and a minimum value of 0.062 W/m*K and only a 5% deviation. While considering the mechanical strength (detailed in the next section), the addition of the fiber can significantly reinforce the sample, without affecting the insulation property.

3.4 Mechanical characterization

The mechanical strength is characterized to show the durable pore-support structure of the printed sample, using the compression test stand (ESM303, MARK-10, Copiague, NY). As discussed in Section 3.3, fiber is added to the ink for printing, in order to reinforce the strength, the evaluated sample is in cubic shape with a dimension of 10 mm long by 10 mm wide by 10 mm thick. A sample without fiber content is also characterized as a control sample.

The experimental results from Section 3 are correlated to one another, here we will comprehensively discuss all the results.

Comparison of drying methods shows that freeze-drying procedure takes the longest time, but the resulting thermal conductivity is not outperforming the ambient pressure drying, meaning the time cost can be saved by 56% if using the proposed ambient pressure drying. With the consideration of expensive equipment costs of freeze drying, the actual cost-saving is

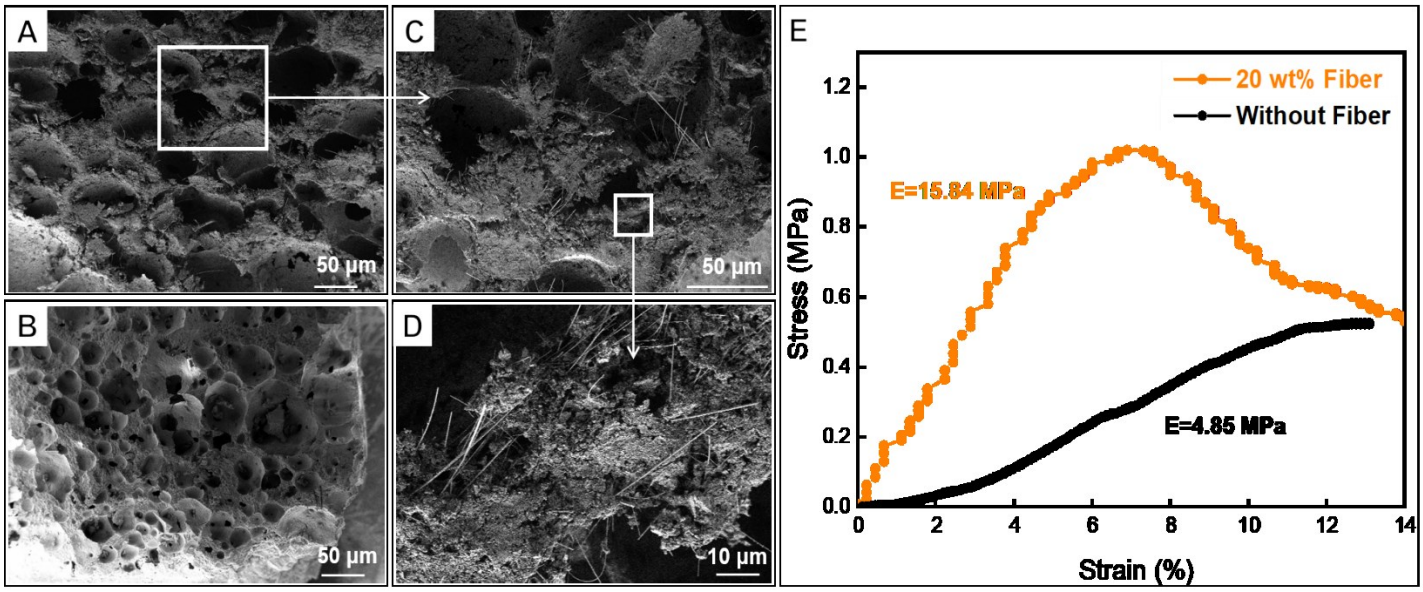

FIGURE 4: Microstructure and mechanical properties characterization. A-B) The internal porous structures. C) Silica aerogel combined with fiber content. C) Bonding of fiber and aerogel skeleton. E) Stress-Strain curves for specimens without fiber and with 20 wt.% fiber content.

The Stress-Strain curve is shown in figure 4(E), the control sample has a Young's modulus of 6.5 Mpa with a maximum load of 0.52 Mpa. While with the addition of fiber, the sample has a Young's modulus of 15.84 Mpa with a maximum load of 1.02 Mpa. Young's modulus as a mechanical property that measures the stiffness of the sample, is 3 times stronger than without fiber content, which concludes that the fiber is effective in reinforcing the sample strength.

3.5 Characterization of the microstructure

The microstructure of the printed sample, as illustrated in figure 4 (A-D), is characterized by scanning electron microscopy (SEM). Figure 4 (A) shows the evenly distributed pore structures, zoomed in to (C) demonstrates pores with combined fiber contents. (D) shows the fiber bonds well with the aerogel skeleton, which substantially contributes to the increased structural strength.

4. DISCUSSION

substantial. For the sintering drying method, although it is widely used for direct ink writing [23, 24] to help remove all the organic solvent and additives, it suffers from the potential internal cracks during and after sintering, which requires adding the additives, such as binder to help prevent the structure from collapse. Furthermore, the sintering process also requires precise temperature control, which will incur considerable equipment cost. Considering manufacturing the aerogel products, neither of the freeze drying or sintering could be an effective way. For the ambient pressure drying, which also results in good thermal insulation performance, but it does not require heavy equipment investment, and the processing time is relatively short, which makes it promising towards the large-scale and low-cost fabrication.

The mechanical strength is another important property for the aerogel products. Since aerogel has a highly-porous structure, the majority of the internal structure is in the form of empty shells. Therefore, the binding of the aerogel skeleton is critical to make durable structures. Here, in order to reinforce the strength but not affect the thermal insulation performance, fiber content is added to the ink. The mechanical test shows that after adding fiber it has a 143% increase in Young's modulus, which means the fiber plays a vital role in making the sample much

stiffer. The investigation of the microstructure by SEM confirms that the samples have uniform internal porous structure and the fiber contents bind well with the skeleton. The blending procedures (Section 2.1) is of critical importance for the good binding. Blending facilitates the relative long fiber content evenly dispersed in the ink without settling down or tangling together. It should be pointed out that after printing, the fiber is located along the longitudinal direction since the printing is done by extruding cylindrical filament and printed layer by layer. After drying, the small, scattered fiber will tangle together, and form a stiff structure and therefore enhance the overall strength. On the other hand, the pore-supporting skeleton is another factor to foam a durable structure. As introduced in the Section 1, the gaseous bubbles in the ink eventually well-developed into the pores after drying. From the SEM images in Figure 4, no crack has been observed even at a microscale level. This concludes that the pore-supporting structure, together with the addition of the fiber content can make the printed sample strong and durable.

The process parameter study provides a guideline on how to further optimize the fabrication with respect to the thermal insulation performance. It can be concluded that with lower infill density, the sample can reach a better performance of thermal conductivity and it proved that direct ink writing is a feasible way to produce the aerogels. While 50% infill density is the lowest reached for this study, it could be further decreased by designing the internal truss-like structures. Not only it can reach ever lower infill density but also the truss-like structure is proven to be a rigid structure. For the foaming agent, it helps to generate in-situ pores, but the amount shall be controlled. The study shows a 0.5% CTAB concentration performs worse than the 0.3% concentration, primarily due to the over-generated bubbles tend to merge together to form undesired large bubbles. Currently, the proposed approach is limited in controlling the pore size. Ideally, all the pore size should be less than 60 nm in order to perform a better thermal insulation behavior. While the current pore is ranging from 20 – 100um. For the future improvement, the better method to control of pore size can be explored from the foam ink preparation step. Based on the density of the current sample and the benchmark samples with lower thermal conductivity, they have the same level of density, which means the foaming agent content is sufficient to introduce the gaseous bubbles. However, after the bubbles are formed, a better approach of blending in order to achieve smaller pore size shall be used to replace the current method.

5. CONCLUSION

In summary, a cost-effective approach to direct write 3D printable aerogel ink is demonstrated. The fabrication method is enabled through the development of gaseous bubbles silica aerogel ink and the direct ink writing setup. Further, combining with the ambient pressure drying after printing, the samples achieve both thermal insulation property and durable mechanical strength. From a manufacturing perspective, the DIW method is capable of customizing different geometry depending on applications. From a large-scale production perspective, this approach is scalable and cost-effective compared to the conventional approach to produce insulation aerogels.

ACKNOWLEDGMENTS

The authors would like to gratefully acknowledge the support from the National Science Foundation (NSF) through CMMI-1846863 and U.S. Department of Energy, Office of Energy Efficiency and Renewable Energy through DEEE-0008675. We thank Dr. Mark Swihart, Dr. Jason Armstrong, Dr. Donghui Zhao and Moein Mohammadi for the scientific discussions. The fiber sheet was kindly provided to us by Unifrax Inc.

REFERENCES

1. Acharya, A., D. Joshi, and V.A. Gokhale, *AEROGEL—a promising building material for sustainable buildings.* Chemical and Process Engineering Research, 2013. **9**: p. 1-6.
2. Riffat, S.B. and G. Qiu, *A review of state-of-the-art aerogel applications in buildings.* International Journal of Low-Carbon Technologies, 2012. **8**(1): p. 1-6.
3. Fesmire, J.E., *Aerogel insulation systems for space launch applications.* Cryogenics, 2006. **46**(2-3): p. 111-117.
4. Yang, J., et al., *Cellulose/graphene aerogel supported phase change composites with high thermal conductivity and good shape stability for thermal energy storage.* Carbon, 2016. **98**: p. 50-57.
5. Dorcheh, A.S. and M. Abbasi, *Silica aerogel; synthesis, properties and characterization.* Journal of materials processing technology, 2008. **199**(1-3): p. 10-26.
6. Leventis, N. and C. Leventis, *Methods and compositions for preparing silica aerogels*. 2010, Google Patents.
7. Industrial, A.A. *High Temperature Insulation – Pyrogel XTE*. 2019; Available from: https://www.aerogel.com/products-and-solutions/pyrogel-xte/default.aspx.
8. CabotCorporation. *Aerogel Products*. 2019; Available from: http://www.cabotcorp.com/solutions/products-plus/aerogel.
9. Aerogel.org. *Strong and Flexible Aerogels*. 2018; Available from: http://www.aerogel.org/?p=1058.
10. Van Bommel, M. and A. De Haan, *Drying of silica aerogel with supercritical carbon dioxide.* Journal of Non-Crystalline Solids, 1995. **186**: p. 78-82.
11. Guo, X., et al., *Facile Synthesis of Methylsilsesquioxane Aerogels with Uniform Mesopores by Microwave Drying.* Polymers, 2019. **11**(2): p. 375.
12. Hu, W., et al., *Preparation of hydrophobic silica aerogel with kaolin dried at ambient pressure.* Colloids and Surfaces A: Physicochemical and Engineering Aspects, 2016. **501**: p. 83-91.
13. Zhang, Q., et al., *3D printing of graphene aerogels.* Small, 2016. **12**(13): p. 1702-1708.
14. Yang, F., et al., *Phase change materials (PCM) based cold source for selective freezing 3D printing of porous*

materials. The International Journal of Advanced Manufacturing Technology, 2018. **95**(5-8): p. 2145-2155.
15. Zhao, G., et al., *Thermal analysis of directional freezing based graphene aerogel three-dimensional printing process.* 2017. **5**(1).
16. Zhao, G., et al., *Tool Path Planning for Directional Freezing-Based Three-Dimensional Printing of Nanomaterials.* 2018. **6**(1).
17. Zhang, F., et al., *Parameter study of three-dimensional printing graphene oxide based on directional freezing.* 2017. **139**(3).
18. Maleki, H., et al., *Compressible, Thermally Insulating, and Fire Retardant Aerogels through Self-Assembling Silk Fibroin Biopolymers Inside a Silica Structure—An Approach towards 3D Printing of Aerogels.* ACS applied materials & interfaces, 2018. **10**(26): p. 22718-22730.
19. Muth, J.T., et al., *Architected cellular ceramics with tailored stiffness via direct foam writing.* Proceedings of the National Academy of Sciences, 2017. **114**(8): p. 1832-1837.
20. M'barki, A., L. Bocquet, and A. Stevenson, *Linking rheology and printability for dense and strong ceramics by direct ink writing.* Scientific reports, 2017. **7**(1): p. 6017.
21. Song, X., et al., *Biomimetic 3D Printing of Hierarchical and Interconnected Porous Hydroxyapatite Structures with High Mechanical Strength for Bone Cell Culture.* Advanced Engineering Materials, 2019. **21**(1): p. 1800678.
22. Liu, J., et al., *Effects of pore structure on thermal conductivity and strength of alumina porous ceramics using carbon black as pore-forming agent.* Ceramics International, 2016. **42**(7): p. 8221-8228.
23. Nan, B., et al., *Direct ink writing of macroporous lead‐free piezoelectric Ba0. 85Ca0. 15Zr0. 1Ti0. 9O3.* Journal of the American Ceramic Society, 2019. **102**(6): p. 3191-3203.
24. Zhou, N., et al., *Gigahertz Electromagnetic Structures via Direct Ink Writing for Radio‐Frequency Oscillator and Transmitter Applications.* Advanced Materials, 2017. **29**(15): p. 1605198.